Measurement-based characterization of 15 GHz propagation channels in a laboratory environment

Yin, Xuefeng; Ji, Yilin; Yan, Hua

Published in:
IEEE Access

DOI (link to publication from Publisher):
10.1109/ACCESS.2017.2657739

Publication date:
2017

Document Version
Publisher's PDF, also known as Version of record

IEEE Access
Multidisciplinary | Rapid Review | Open Access Journal

Received December 22, 2016, accepted January 12, 2017, date of publication January 25, 2017, date of current version March 13, 2017.

Digital Object Identifier 10.1109/ACCESS.2017.2657739

Measurement-Based Characterization of 15 GHz Propagation Channels in a Laboratory Environment

XUEFENG YIN[1], YILIN JI[2], AND HUA YAN[3]
[1]College of Electronics and Information Engineering, Tongji University, Shanghai 201804, China
[2]Department of Electronics System, Aalborg University, DK-9220 Aalborg, Denmark
[3]Huawei Technologies Co., Ltd., Chengdu 610041, China

Corresponding author: X. Yin (yinxuefeng@tongji.edu.cn)

This work was supported in part by the Key Project 5G Ka Frequency Bands and Higher and Lower Frequency Band Cooperative Trail System Research and Development through the China Ministry of Industry and Information Technology under Grant 2016ZX03001015, in part by the Hong Kong, Macao and Taiwan Science and Technology Cooperation Program of China under Grant 2014DFT10290, in part by the Key Program of National Natural Science Foundation of China (NSFC) under Grant 61331009, in part by the NSFC General Project under Grant 61471268, and in part by the Project Measurement-based space-time channel modeling for 5G Wireless Communication of Huawei Technology Company.

ABSTRACT In this paper, measurements in a laboratory characterizing the 15-GHz band propagation channels are introduced. Both an omnidirectional antenna (ODA) and a 10° half-power-beamwidth (HPBW) pyramidal horn antenna are deployed at the transmitter (Tx) in different measurements. The receiver (Rx) is equipped with a 10° HPBW horn antenna. A direction-scanning sounding method is applied by rotating the Rx horn antenna in steps of 5° to collect channel impulse responses (CIRs) in the angular domains. Clusters are extracted based on power concentration from the 3-D power spectrum in delay, azimuth, and zenith arrival angles. Each cluster represents the contribution of specular paths with similar delay, azimuth, and zenith arrival angles, and of the diffuse-scattering components spreading around these paths. The mapping of the propagation paths reconstructed from the extracted clusters to the physical interacting objects in the environment is found to be reasonable. Differences on channel characteristics are compared for both a horn antenna and an ODA at the Tx. Finally, a stochastic cluster model is provided based on five measurements in the laboratory for the case where the ODA is used at the Tx.

INDEX TERMS Higher frequency band propagation, direction-scanning sounding, small scale characterization, clustering, diffuse scattering.

I. INTRODUCTION

The rapid growth of the increasing demand in data rate for the fifth generation (5G) communications prompts the motivation for designing communication systems on higher frequency bands (HFBs) beyond 6 GHz because of abundant spectrum resources potentially available [1]–[3]. Conventionally, wireless communications in HFBs were mainly for backhaul transmissions, and thus, characterization of channels above 6 GHz has been focusing on narrowband properties and profile/composite characteristics, such as fading, rain attenuation, and shadowing. The fast-developing 5G stimulates the studies on wideband characteristics of HFB channels, particularly the delay and spatial perspectives in various propagation scenarios [2], [4]. Numerous channel measurements have been conducted in HFBs, such as the centimeter (cm-) wave bands at 10 GHz [5], 11 GHz [6], [7], 20 GHz [55], 28 GHz [8]–[12], [57], and millimeter (mm-) wave bands such as the 38 and 60 GHz [5], [16]–[18], the 70-73 GHz [19]–[23], [57], and the 81-86 GHz [21]. A series of channel models have been proposed in these works, which include large-scale path loss models [6], [8], [11], small-scale channel impulse response models in form of the Saleh-Valenzuela model [12], [40] and of the multipath-cluster 3GPP spatial channel model [12]–[15], [20], [54]. The results obtained illustrate both the pros and cons of using HFBs for wireless transmission in indoor and outdoor scenarios [24]. For example, the path loss at 28 GHz was found to maintain reasonable levels, with the path loss exponent (PLE) equal to 2.55 for line-of-sight (LoS) scenarios and 4.58 for none-line-of-sight (NLoS) scenarios, which

allow communications between the user equipment (UE) and the base station (BS) even when they are separated by 200 meters [8]. Recently, exploring the HFBs for cm-wave receives increased attentions. Ericsson and NTT Docomo announced their experimental results of achieving 5 Gbps high-data-rate communication by using 15 GHz frequency bands [25]. The coverage of a communication network can be more wide and robust for using the cm-wave than the mm-wave. Meanwhile, the bandwidth of the signal transmission when the cm-wave is adopted can be kept similar with that applied in mm-wave. Therefore, channel characterization for HFBs of cm-wave is of interest to investigate.

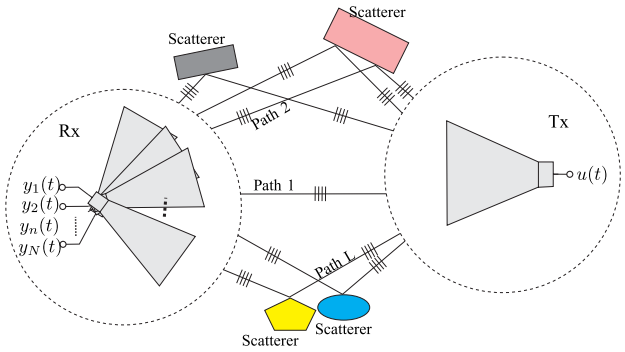

Fig. 1. The measurement approach adopted in the campaign, where $u(t)$ is the sounding signal, and $y_n(t)$, $n = 1, \ldots, N$ are the received signals at N different Rx orientations.

In HFB channel measurements, horn antennas with directional radiation patterns are widely used [12], [19], [26], [27], [55]. A motivation for using horn antennas is that the high antenna gains can compensate the propagation attenuation in HFBs. In the case where the horn antenna's half-power beamwidth (HPBW) is small, the antenna needs to be rotated mechanically in order to cover specific ranges of directions. Thus, a so-called ''omni-to-omni (O2O)'' channel originally observed by using omnidirectional antennas (ODAs) at the Tx and Rx can be reconstructed by multiple ''directional-to-directional (D2D)'' channels obtained by scanning the direction of departure (DoD) and direction of arrival (DoA) domains stepwise with horn antennas. Fig. 1 illustrates a diagram of direction-scanning channel sounding with the Tx antenna fixed and the boresight of the Rx antenna is oriented following a pre-defined scanning procedure. Another motivation of using horn antennas, especially those with narrower HPBWs in channel sounding is that the angular resolution, i.e. the minimum resolvable spacing among multipath components (MPCs) in the angular domains, is approximately equal to the HPBW which can be significantly superior to that achieved by using multi-element arrays as in the case of e.g. 3GPP and WINNER channel modelling [28]–[30].[1]

[1]According to [31, Eq. (2)], the resolution in e.g. azimuth can be calculated to be $360/(N\pi)$ in degree approximately, where N is the number of antennas in a uniform linear array with neighbouring antennas spaced by $1/2$ wavelength. In order to fulfil the small-scale characteristic assumption [32], N needs to be kept small, e.g. not exceeding 7. It can be calculated that the resolution is always above 16.37° for arbitrary $N \leq 7$.

From the modelling point of view, it is necessary to provide an O2O channel model which can be used to generate D2O and D2D channels for specific scenarios in 5G communications. An interesting issue arising for channel measurements using direction-scanning is that whether it is possible to synthesize an O2O channel based on measured D2D channels, and how to do it effectively. Recently, it was shown in [33] that the narrowband properties, such as path loss of a channel observed with a flat omnidirectional-like antenna radiation pattern can be obtained via integrating multiple channels measured by rotating a directional antenna, provided the rotation step equals the antenna's HPBW. The differences of the so-called wideband characteristics, e.g. the delay and directional dispersion of MPCs grouped as clusters, have not been investigated for D2O and O2O channels so far [55], [56]. A detailed characterization of HFB channels in different scenarios is important for system design when beamforming techniques are implemented at, for example, the base stations.

In this contribution, we introduce a recently conducted measurement campaign for channel characterization of wave propagation at 15 GHz band in a laboratory. The measurements were conducted through direction-scanning sounding with the receiver (Rx) equipped a 10° HPBW antenna rotated in azimuth of arrival (AoA) and zenith of arrival (ZoA). In order to understand the impact of directivity of Tx antenna on propagation, measurements were conducted while the Tx is equipped with either an omnidirectional biconical antenna or a directional antenna with 10° HPBW. Clusters are extracted from the channel power spectrum in three dimensions, i.e. delay, AoA and ZoA. The center of such a cluster coincides with a local maximum of the spectrum, and the spread of the cluster is caused jointly by closely-spaced MPCs and diffuse-scattering, as well as measurement system responses that are not de-embedded from the measured CIRs. The propagation mechanism is investigated by mapping the extracted clusters to the physical interacting objects in the environment considered. Statistical characteristics of power in delay, AoA and ZoA are presented and compared among different propagation scenarios.

The paper is organized in the following manner. Section II describes the measurement campaign, the laboratory environment and the antenna configurations considered. Section III elaborates the proposed cluster extraction method and defines the parameters' characteristics of the clusters. Section IV describes the measurement results for the differences between O2O and D2O channels, and cluster-to-object mapping. Section V presents the statistics of the cluster characteristic parameters extracted from five measurements in the laboratory. Finally, conclusive remarks are given in Section VI.

II. MEASUREMENT ENVIRONMENT AND SETUP

The measurements were conducted in a laboratory of the Physics department in Tongji University. A Vector Network Analyzer (VNA) of the type ''Agilent 8722ES'' was used

Fig. 2. A photograph of the laboratory where measurements are conducted.

for signal transmitting and receiving.[2] Fig. 2 illustrates a picture of the laboratory. There were two locations for the Tx of height 2.4 meters and 1.5 meters respectively, and three locations for the Rx of height equal to 1.5 meters. All these locations were in the laboratory. A direction-scanning sounding scheme described in Fig. 1 was applied during the measurements. In order to investigate the distinctions of D2O channel and O2O channel, a bi-conical omnidirectional antenna and a horn antenna of 10° HPBW were used at the Tx in different measurements respectively. When the horn antenna was mounted at the Tx, the boresight direction of the Tx horn was pointed directly towards the Rx's location along the line-of-sight (LoS) direction. In the Rx side, a horn antenna of 10° HPBW was used. The boresight of the Rx horn antenna was rotated in the step size of 5° in the AoA from 0° to 360°, where 0° corresponds to the azimuth of the LoS direction, and the ZoA ranging from −30° to 30°, where 0° corresponds to the zenith of the horizontal plane. This resulted in 72 steps in azimuth and 13 steps in zenith, and consequently $13 \times 72 = 936$ channel impulse responses were obtained for each measurement. The room was in the dimension of $10 \times 6.5 \times 3.3$ m^3 and surrounded with glass windows. Many equipments were placed on tables during measurements.

It can be found from recent literature which introduce channel measurements using direction-scanning approaches that a horn antenna is usually rotated in the step size identical to the antenna's HPBW. This is necessary since the overall received power in an omnidirectional channel can be approximated by summing up the signals' powers received at individual channels not overlapped in directions. In our case, we are interested at the distribution of channel components in directions, rather than the overall channel gain. With a smaller step size in scanning a channel, more refined characteristics can be observed, which is analogous to interpolating the channel spread function with denser samples. In the measurements considered here, the Rx antenna was stepped in both azimuth and zenith at 5°, which is half of the HPBW of the underlying horn antenna [34], [35].

[2]The VNA has been widely used for propagation channel measurements. Some examples can be found in [51]–[53].

TABLE 1. Specifications of the horn antenna and the biconical omnidirectional antenna used in the measurement, and the corresponding VNA settings.

Specifications	10° HPBW horn antenna	Biconical omni-directional antenna
Frequency Range (GHz)	10-17	2-30
Gain at 15 GHz (dBi)	25	4
H-plane HPBW (°)	10°	360°
E-plane HPBW (°)	10°	10°
Polarization	Vertical	Vertical
	Measurement settings for the VNA	
Frequency span	14–17 GHz	
Resolution Bandwidth (RBW)	3 KHz	
Transmission power	−10 dBm	
Number of sweep points	1601	

Table 1 lists the specifications of the antennas and the VNA settings. The measurements were conducted with a chirp signal of frequency ranging from 14 GHz to 17 GHz. Channel responses at totally 1601 frequency points were recorded, which were further processed using inverse Fourier transformation to generate the channel impulse response of 1601 delay samples. The environment was kept stationary without objects and human moving during the measurements.

III. CLUSTER EXTRACTION AND PARAMETER CALCULATION

It is conventional for channel modelling that the propagation channel can be viewed as a superposition of MPCs [31], [36]. In the direction-scanning sounding scenarios, the propagation paths can be extracted directly by localizing the peaks of the CIR magnitude for the high delay and angular resolutions benefitted from the wide bandwidth of the sounding signal and the underlying directional antenna of narrow beam, respectively. This channel analysis approach can be called ''non-parametric'', and similar analysis has been widely conducted for HFB and mm-wave channel characterization e.g. in [5], [6], [8]–[12], [16]–[24]. In our case, we focus on the small-scale characterization represented in terms of multiple clusters extracted via non-parametric approaches. A simple and robust method is proposed in the following which is used to extract the clusters from the measured delay-AoA-ZoA power spectrum.

A. CLUSTER EXTRACTION

Let us denote the delay-AoA-ZoA channel power spectrum with $P(\mathbf{\Omega})$ where $\mathbf{\Omega} = [\tau, \phi, \theta]^{\mathrm{T}}$ is a vector containing the variables in delay τ, AoA ϕ and ZoA θ, and $(\cdot)^{\mathrm{T}}$ represents the transpose operation. From the measured impulse response $h(\mathbf{\Omega})$, $P(\mathbf{\Omega})$ can be calculated as

$$P(\mathbf{\Omega}) = |h(\mathbf{\Omega})|^2. \tag{1}$$

In measurements, the variables in $\mathbf{\Omega}$ are discretized as follows: $\tau \in [n/B; n = 0, \ldots, N-1]$ are the delay samples where N represents the total number of samples and B the

signal bandwidth, $\phi \in [m2\pi/M; m = 0, \ldots, M-1]$ are the azimuths of Rx antenna boresight with M being the total steps in AoA, and $\theta \in [l(\theta_e - \theta_s)/(L-1) + \theta_s; l = 0, \ldots, L-1]$ stands for the zenith angle of Rx antenna boresight with θ_s and θ_e being the starting and the ending zeniths respectively, and L the total number of steps in ZoA. In the cases considered here, $P(\mathbf{\Omega})$ is measured with 1601 samples in delay, 72 samples in AoA and 13 samples in ZoA. Thus, an overall 936 ($= 72 \times 13$) directions are scanned for a channel. The neighbouring samples in delay are separated by 0.33 ns, corresponding to a range resolution of 1 cm, and the consecutive samples in the AoA and ZoA are separated by 5°.

Under the assumption that the propagation channel is a superposition of the clusters and the noise component, $P(\mathbf{\Omega})$ can be rewritten as

$$P(\mathbf{\Omega}) = \sum_{i=1}^{I} P_i(\mathbf{\Omega}) + P_n, \tag{2}$$

where I is the total number of clusters, P_n represents the noise spectral height, and $P_i(\mathbf{\Omega})$ denotes the power distribution of the ith cluster composed of MPCs located in a set $\boldsymbol{s}_i$ of $\mathbf{\Omega}$. Individual clusters $P_i(\mathbf{\Omega})$, $i = 1, 2, \ldots, I$ are extracted sequentially from $P(\mathbf{\Omega})$ with the following three steps:

Step 1 (Determine the Location of the ith Cluster): Find the location of $\mathbf{\Omega}$ where the maximum of $P(\mathbf{\Omega})$ is identified. Denote the location with $\boldsymbol{s}_i^{\mathrm{p}}$, and consider it to be the peak of the ith cluster where the strongest power is observed.

Step 2: Group the samples in the vicinity of $\boldsymbol{s}_i^{\mathrm{p}}$ as a cluster. Practically, the "vicinity" is set to a rectangular-shaped region, denoted with $\boldsymbol{s}_i^{\mathrm{v}}$, which is centered at $\boldsymbol{s}_i^{\mathrm{p}}$ with a length of $2\beta_\tau$ in delay, $2\beta_\phi$ in AoA, and $2\beta_\theta$ in ZoA respectively. Here, β_τ, β_ϕ and β_θ, which can be represented in samples in their corresponding dimensions, are determined based on a certain criterion to be discussed later in this section. Any sample with its location $\boldsymbol{s}$ within the region $\boldsymbol{s}_i^{\mathrm{v}}$ is assigned to the ith cluster if and only if its power, represented by P_s, is above a threshold α in dB added to the noise spectral height P_n, i.e. $\{\boldsymbol{s} \in \boldsymbol{s}_i : \boldsymbol{s} \in \boldsymbol{s}_i^{\mathrm{v}} \ \wedge \ P_s \geq P_n + \alpha\}$, where P_s and P_n are represented in dB. The objective of setting α is to extract the dominant portion of the cluster and meanwhile, suppress the contribution of noises. Later on in Section III-B, an empirical approach for determining the value of α will be elaborated for the specific case considered in our work. When calculating the distance between $\boldsymbol{s}$ and $\boldsymbol{s}_i^{\mathrm{p}}$ in AoA, the cyclic behavior at $\phi = 360°$ and 0° needs to be considered. A simple method to find the exact distance between two samples in AoA, say ϕ_1 and ϕ_2, is calculated as

$$\Delta\phi = \begin{cases} (360° - \tilde{\phi})/\phi_{\mathrm{step}}, & \text{for } \tilde{\phi} > 180° \\ \tilde{\phi}/\phi_{\mathrm{step}}, & \text{for } \tilde{\phi} \leq 180° \end{cases} \tag{3}$$

with $\tilde{\phi} = \phi_1 - \phi_2$ and $\phi_{\mathrm{step}} = 5°$ being the rotation step in AoA in our case.

Step 3 (Remove the ith Cluster Extracted, and Find the Next Cluster Successively): All the samples assigned in the ith cluster are removed from $P(\mathbf{\Omega})$. Then, the operation in *Step 1* is re-executed to find the $(i+1)$th cluster.

Steps 1-3 can be applied iteratively until the maximum power of a new cluster is below $P_n + \alpha$ dB. An advantage of this simple method is that the number of clusters does not need to be pre-determined. With adaptive setting for the number of clusters, we can exhaustively extract all dominant components in the channel and meanwhile, avoid including any insignificant samples subject to the noise contribution.

It is worth mentioning that instead of the directional cosine adopted in e.g. [37] for calculating the so-called multipath component distance (MCD) [38], the distance in observation samples is used as the measure of difference between two measurement samples. This is mainly because the measurement samples are not exactly the conventionally defined MPCs, and the extraction of the clusters can be done straightforwardly in this way in three sampling dimensions, i.e. delay, AoA and ZoA. It must be noticed that the measurement data is indeed the convolution result between the real propagation channel power spectrum and the horn antenna radiation pattern, which means that the measured delay-AoA-ZoA power spectrum is just an approximation of the pure channel power spectrum. Nonetheless, with high measurement system resolution, i.e. horn antennas of small HPBW and ultra-wide bandwidth sounding signals, the measured power spectrum would approach the real one and can be used for small-scale characterization in both angles and delay. In this context, the extracted clusters are the MPCs convolved with the antenna pattern together with the diffuse scattering.

B. DETERMINING α AND β

The parameters β and α determine the extension of a cluster and the noise threshold level respectively. In our case, each cluster is assumed to have only one or several unresolvable closely spaced MPCs together with the surrounding diffuse scattering. Figs. 3(a) and 3(b) illustrate respectively the marginal angular power spectrum of an O2O channel and the power delay profile of a O2D channel measured with the Rx horn antenna's main beam directed towards the Tx omni-directional antenna. A grid in Fig. 3 (a) represented in "samples" equals 5° in both azimuth and zenith, and the circles in Fig. 3 (b) indicate the delay samples of power above the threshold $P_n + \alpha$. The interval between two consecutive delay samples is 0.33 ns which is calculated as the inverse of the signal bandwidth 3 GHz in the case considered here. It can be observed from Fig. 3 (a) that a lobe of the power spectrum with a single maximum is confined within approximately 10 samples in azimuth and 10 samples in zenith. Similarly, in the delay domain a single lobe is observed to have an extension less than 10 samples. Based on those visual inspections, we selected $\beta_\tau = \beta_\theta = \beta_\phi = 5$ samples for the maximum scopes of a cluster in all considered three dimensions. Specifically, the diameter of a cluster in our case is limited by 3.33 ns in delay, and 50° in both azimuth and zenith. Notice that the selection of 5 samples as the maximum extension of a cluster in all three dimensions is merely a

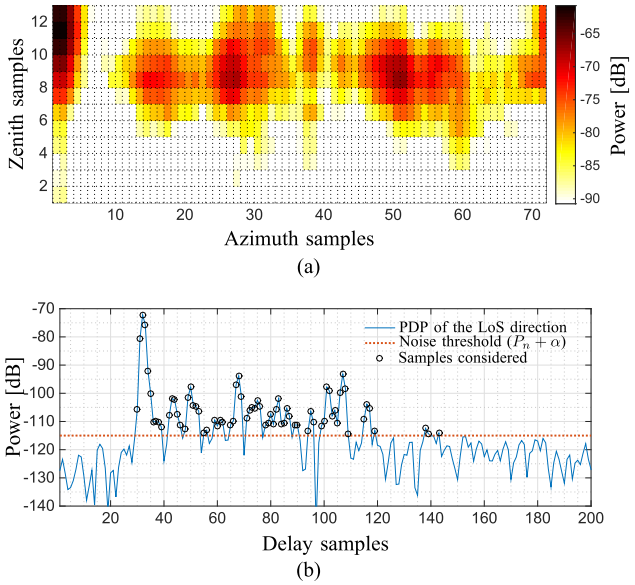

Fig. 3. (a) Marginal angular power spectrum of the O2O channel and (b) the power delay profile (PDP) of its strongest direction, i.e. the LoS direction.

coincidence in the case considered. These thresholds can be set differently, depending on both the resolution of the measurement equipment and the exact dispersion of a channel in the dimensions concerned. Furthermore, $\alpha = 5$ dB is selected in our case, which effectively avoids the problem of overestimating cluster spreads caused by involving noise components in clusters.

It is worth mentioning that a drawback of fixing the maximum cluster scope for extracting clusters is that the power spectrum of a cluster obtained may exhibit multiple local power maxima, which does not follow the definition in [39] that a cluster exhibits only one power maximum. However, our experience also showed that applying the "single-power-maximum cluster" definition would lead to a large amount of clusters, especially for the HFB channels measured in our case with the relatively dense direction-scanning and with several GHz bandwidth. Comparing to the method of identifying single-power-maximum clusters, we found that our proposal of cluster extraction method with limited cluster extensions leads to tractable modelling complexity, and thus more appropriate to adopt in the analysis conducted here.

C. PARAMETERS OF A CLUSTER

The center of gravity $\bar{\mathbf{\Omega}}_i$ of the ith cluster can be calculated as the first moment of $\mathbf{\Omega}$, i.e.

$$\bar{\mathbf{\Omega}}_i = \int_{s_i} \mathbf{\Omega}\, p_i(\mathbf{\Omega}) d\mathbf{\Omega}, \tag{4}$$

where the normalized power spectral density $p_i(\mathbf{\Omega})$ reads

$$p_i(\mathbf{\Omega}) = \frac{P_i(\mathbf{\Omega})}{P_i} \tag{5}$$

with $P_i = \int_{s_i} P_i(\mathbf{\Omega}) d\mathbf{\Omega}$ representing the total power of the $i$the cluster. The covariance matrix $\mathbf{\Sigma}_{\mathbf{\Omega}_i}$ can be estimated with the second central moment of $\mathbf{\Omega}$, which is denoted as $\hat{\mathbf{\Sigma}}_{\mathbf{\Omega}_i}$ and derived as

$$\begin{aligned}\hat{\mathbf{\Sigma}}_{\mathbf{\Omega}_i} &= \int_{s_i} (\mathbf{\Omega} - \bar{\mathbf{\Omega}}_i)(\mathbf{\Omega} - \bar{\mathbf{\Omega}}_i)^{\mathrm{T}} p_i(\mathbf{\Omega}) d\mathbf{\Omega} \\ &= \begin{bmatrix} \sigma_{\tau_i}^2 & \rho_{\tau_i\phi_i}\sigma_{\tau_i}\sigma_{\phi_i} & \rho_{\tau_i\theta_i}\sigma_{\tau_i}\sigma_{\theta_i} \\ \rho_{\phi_i\tau_i}\sigma_{\phi_i}\sigma_{\tau_i} & \sigma_{\phi_i}^2 & \rho_{\phi_i\theta_i}\sigma_{\phi_i}\sigma_{\theta_i} \\ \rho_{\theta_i\tau_i}\sigma_{\theta_i}\sigma_{\tau_i} & \rho_{\theta_i\phi_i}\sigma_{\theta_i}\sigma_{\phi_i} & \sigma_{\theta_i}^2 \end{bmatrix}, \end{aligned} \tag{6}$$

where σ_{τ_i}, σ_{ϕ_i}, σ_{θ_i} are respectively the delay spread, AoA spread and ZoA spread of the ith cluster, and the correlation coefficients between them are denoted with $\rho_{\tau_i\theta_i}$, $\rho_{\tau_i\phi_i}$, $\rho_{\phi_i\theta_i}$.

The calculations in (4) and (6) are performed by taking into account the power spectrum being cyclic in the AoA domain. Furthermore, it is worth mentioning that the AoA spread σ_{ϕ_i} and ZoA spread σ_{θ_i} are different from the directional spread defined in [36] which provides more accurate characterization for power dispersion in angular domains. However, in cases where a cluster is highly concentrated, the directional spread can be approximated by angular spread in radian [36]. As will be shown later in Sect. IV, all clusters extracted from our measurements in multiple scenarios exhibit angular spreads less than 10°, and thus, σ_{ϕ_i} and σ_{θ_i} calculated from (6) approximate the direction spreads closely.

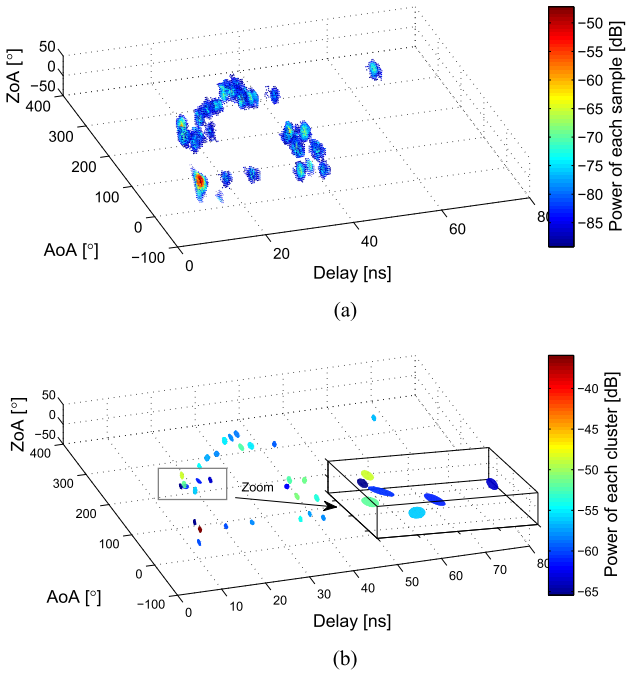

Fig. 4. (a) The extracted 30 strongest clusters and (b) the corresponding reconstructed Gaussian distributions for one of the measured O2O channels.

As an example, Fig. 4(a) depicts 30 strongest clusters in the delay, AoA, and ZoA domains, extracted from one of the measured O2O channels, where the colors of the spots code the power in decibel. Fig. 4(b) illustrates the ellipsoids that coincide with the 3-D surfaces where $\mathbf{\Omega}$ satisfies the equality $(\mathbf{\Omega} - \bar{\mathbf{\Omega}}_i)^{\mathrm{T}} \Sigma_{\mathbf{\Omega}_i}^{-1} (\mathbf{\Omega} - \bar{\mathbf{\Omega}}_i) = 1$, $i = 1, \ldots, 30$. In the case where $\rho_{\phi_i\theta_i}$, $\rho_{\phi_i\tau_i}$ and $\rho_{\phi_i\theta_i}$ are close to zeros,

the extension of the ith ellipsoid along the three semi-principal axes approximately equals $2\sigma_{\tau_i}$, $2\sigma_{\phi_i}$, $2\sigma_{\theta_i}$, respectively. A zoom-in look of several certain ellipsoids is plotted in the enlarged 3-D box in Fig. 4(b) for clarity. The colors of the ellipsoids in Fig. 4(b) represent the total power of each cluster P_i. By comparing Figs. 4(a) and 4(b), we can observe that the extracted clusters provide consistent descriptions for the local maxima of the original power spectrum and the extensions of the spectrum around them.

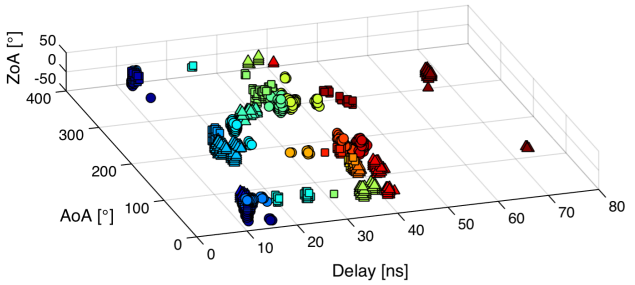

Fig. 5. Measurement samples grouped by using the K-power-means algorithm for the same measurement data in Fig. 4. Samples of both the same colour and shape belong to a single cluster.

D. COMPARED TO THE K-POWER-MEANS CLUSTERING RESULTS

The K-power-means algorithm was widely applied to clustering of estimated MPCs for constructing WINNER-like SCMEs and 3GPP SCMs [39]. In this algorithm, the MCD is utilized as a measure of the separation of two MPCs in multiple dimensions. The path powers are taken into account when calculating the MCD. The K-power-means algorithm iteratively minimizes the summation of the MCDs between the geometrical center of a cluster and all the MPCs assigned to this cluster. The total number of clusters is a parameter of the K-power-means algorithm, which can be pre-determined by adopting certain cluster number validity index, e.g. Calinski-Harabasz (CH) index or Davies-Bouldin (DB) index [39]. Fig. 5 illustrates the clustering result obtained using the K-power-means algorithm to the same measurement data as used for generating the results shown in Fig. 4. The samples in the delay-AoA-ZoA power spectrum with their powers less than 30-dB below the maximum of the spectrum were applied for clustering. In Fig. 5, spots denoted with the same colors and same marks indicate the samples grouped as one cluster. By comparing the result with the reconstructed clusters shown in Fig. 4(b), it is obvious that similar clustering results are obtained by using the proposed method and the K-power-means method. It is worth mentioning that the K-power-means method has an empirical disadvantage that when the number of measurement samples is huge, e.g. over 5000, the cluster number validation process is very time-consuming compared to our proposed method.

IV. CHANNEL CHARACTERISTICS ANALYSES

In this section, the measurement results obtained for O2O channels and D2O channels are presented. The difference between the channels observed in these two scenarios and the relationship between the channels and the directivity of the Tx antenna are investigated by examining their channel power delay profiles (PDP's), and the mapping between clusters and physical objects in the environment where the measurements were conducted.

A. PDP FOR DIRECTIONAL-Tx AND OMNI-Tx CHANNELS

Theoretically, the power delay profile $P(\tau)$ of an O2O channel can be obtained by calculating the marginal of $P(\phi, \theta, \tau)$ as

$$P(\tau) = \int_0^{\pi} \int_0^{2\pi} P(\phi, \theta, \tau) \mathrm{d}\phi \mathrm{d}\theta. \tag{7}$$

However, since each sample of $P(\phi, \theta, \tau)$ contains noise components, the integral operations in (7) increases the noise spectral height for $P(\tau)$ significantly. As a result, the signal-to-noise ratio (SNR) of $P(\tau)$ becomes so small that only LoS component and strong specular components can be observed. To overcome this problem, a threshold (noise floor) of 3 dB is applied to the delay-AoA-ZoA power spectrum to mitigate the influence of noise, i.e. only the power of samples above the threshold are kept while the power of samples below it are set to zero. Then, the marginal power delay profiles are calculated by summing the power spectrum over angular domain. Because of the zero assignment, the PDP breaks where power is close to the noise floor in logarithmic domain, e.g. at the beginning and the tail of the PDP.

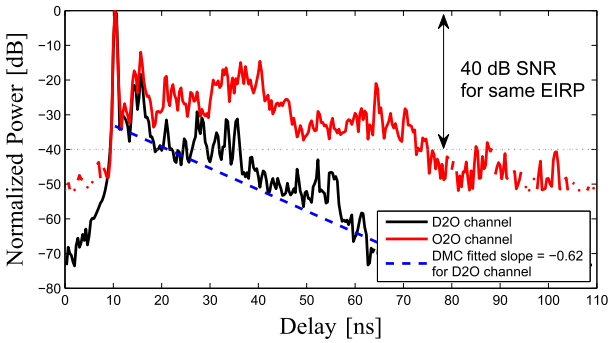

Fig. 6. Comparison of the normalized PDP $P(\tau)$ observed in the D2O channel and the O2O channel.

Fig. 6 shows the normalized PDP for both the D2O channel and the O2O channel. For clarity purpose, the PDPs for one of the measurement location are illustrated as the examples. It can be observed that the SNR is significantly larger for the D2O channel (black solid line) than for the O2O channel (red solid line). This phenomenon is reasonable in the measurement conducted here, since the transmitting antenna has lower gain in the O2O scenario than in the D2O scenario. From Table 1 we can see that the gains of horn antenna and the biconical omni-directional antenna are 25 and 4 dBi respectively. A situation can occur that when the horn antenna transmits, more energy is concentrated in the direction along which the antenna points towards than in the case where the omni-directional antenna is applied. When some paths'

DoDs are within the region where the directional antenna points, the D2O channel may have significantly higher SNR than the O2O channel. From Fig. 6 it can be observed that the improvement of the SNR is approximately 22 dB, close to the additional gain obtained by using the directional Tx antenna, which is 21 dB according to the specifications given in Table 1. Furthermore, it is interesting to observe from Fig. 6 that the power fluctuation versus the delay observed for $\tau < 20$ ns is similar in both cases. For $\tau > 20$ ns, the relative power of the received signal decreases more slowly for the O2O channel than the D2O channel. Specular components can be observed with larger delays from the PDP of the O2O channel.

By fitting the top of the dominant peaks with exponential decays, we observed that the cluster power-delay time constant Γ in Saleh-Valenzuela models [40] for both D2O and O2O channels are 4.18 ns and 11.07 ns, respectively.[3] Furthermore, if the residual after removing specular components from the PDP is considered to be the Dense Multipath Component (DMC) [41], it can be observed that the DMC is more evident in the D2O channels than in the O2O channels. We observed that the power of the DMC in the D2O channels follows an exponential decay along the delay axis with fitted slope equal to -0.62. It is easy to show that the power-delay time constant of the DMC equals 5.4 ns. However, no clear exponential decay trend is observed for the power-delay variation of the DMC in the O2O channels, which is due to the enhanced richness of MPCs widely spread in delay in the O2O scenarios. We note that these observations of power spectrum exponentially decaying over the delay are quite consistent with those reported in [27] for 60 and 70 GHz wave propagation in large indoor scenarios.

To have a fair comparison with approximately the same effective isotropic radiated power (EIRP) and same SNR, we set a threshold (as plotted in gray dashed line in Fig. 6) to fix the considered SNR at 40 dB. The analyses in the sequel are performed under such equal-EIRP condition where the SNR for both D2O and O2O scenarios are equal to 40 dB[4] The rms delay spread of $P(\tau)$ is calculated to be 12.49 ns for the O2O channel and only 2.66 ns in average for the D2O channels. The effect that delay spreads of D2O channels are significantly less than those of O2O channels by approximately one order of magnitude when the same EIRP is achieved, is due to the reason that the wider the Tx antenna beamwidth, more scatterers which are invisible in the case of narrow Tx antenna can be illuminated and participate in the wave propagation. Consequently, a larger excess delay is resulted for the O2O channel compared with the D2O channels. Such observations are also reported in [42] and [43] for both measurements and ray tracing simulations. Since the coherence bandwidth of channel is inversely proportional to the delay spread, D2O channels have coherence bandwidth significantly larger than the O2O channel. This is consistent with the observations in indoor 72 GHz channel measurements reported in [44].

[3]The curve fitting procedure was conducted as follows: we first choose the values of the PDP local maxima that appear after the delay of the LoS component, and then, a least-square-error approach is adopted to find a straight line which fits the best to these selected power-in-dB versus delay. Then, the range in the abscissa within which the y of the straight line decreases by $20\log_{10} e = 8.69$ dB, is considered to be the cluster power-delay time constant Γ.

[4]The real SNRs for the observed PDPs are actually higher than 40 dB. Here, the dynamic range of 40 dB is selected for determining the dominant portion of PDPs that are applicable for channel characterization.

B. MAPPING BETWEEN CLUSTERS AND PHYSICAL OBJECTS IN THE MEASUREMENT PREMISES FOR DIRECTIONAL-Tx AND OMNI-Tx CHANNELS

To investigate the propagation mechanism and find how objects interact with waves, it is necessary to perform the mapping between clusters in parameter domain and real physical domain for both D2O and O2O channels, which is done in a ray-tracing-like manner here. Based on the clusters existing in delay, AoA and ZoA domains, we first draw a line stemming from the Rx antenna along a direction uniquely determined by the centroid of AoA and ZoA of a cluster calculated with (4). Then, we check whether any objects come across the line based on the digital map of the laboratory. If there is an object across the direction, we then connect the Rx to this object, and further to the Tx. In the case where the total length of this one-bounce link is approximately equal to the distance calculated by multiplying the centroid of delay of the cluster with the speed of light, we consider this link as a reasonable estimate of the propagation path yielding the cluster considered. This simple ray-tracing-like method is applied to reconstructing paths for all clusters extracted from both D2O and O2O channels.

Figs. 7(a) and 7(b) show the examples of the cluster-object mapping results for all clusters extracted in the D2O channel, and for the 30 strongest clusters observed in the O2O channel, respectively. This example corresponds to the case that Tx was put on the top of a metal shelf and Rx on a trolley as shown in Fig. 2. In the omni-Tx scenario as depicted in Figs. 7(b), the scatterers are more widely distributed. By comparing, it seems the constitution of paths for the D2O channel is a subset of the O2O channel, which from another perspective also supports the feasibility of synthesizing an omni channel with multiple directional channels, provided they cover the complete direction range as the omni-Tx does. Furthermore, It can be observed from Fig. 7(c) that except for the LoS path, most of the other paths are found to be single-bounce paths. Such simple propagation constellations are consistent with the prediction made in [2] for HFBs. From this, deterministic ray models such as Ray Tracing, or graph models can be effective to predict path constellation based on a detailed environment description [45]–[47].

V. STATISTICS BASED ON MULTIPLE MEASUREMENTS

Considering that D2O channels can be generated using O2O channel models, we focus on extracting the channel statistics for O2O scenarios based on multiple measurements conducted with Tx and Rx located differently in the same laboratory.

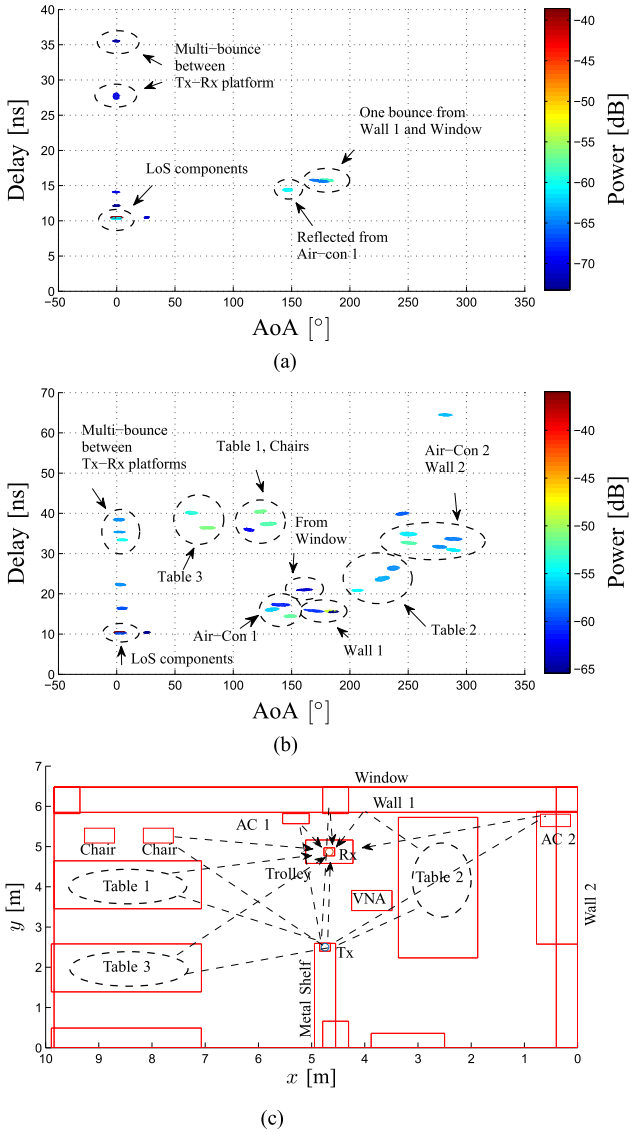

Fig. 7. **The extracted clusters for (a) the D2O channel, and (b) the O2O channel, and (c) the reconstructed paths based on them of the O2O channel.**

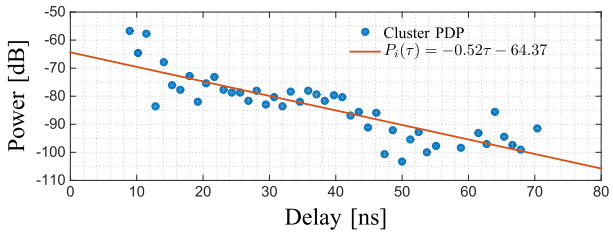

Fig. 8. **Cluster PDP $P_i(\tau)$ and fitted linear equation.**

Fig. 8 depicts the variation of cluster power P_i versus the mean cluster delay. A line parameterized with the slope and the floating intercept at y-axis was fitted to the empirical samples by applying the least mean square error principle. The legend of the figure reports the expression of the fitted line. Fig. 9 and Fig. 10 show the empirical occurrence

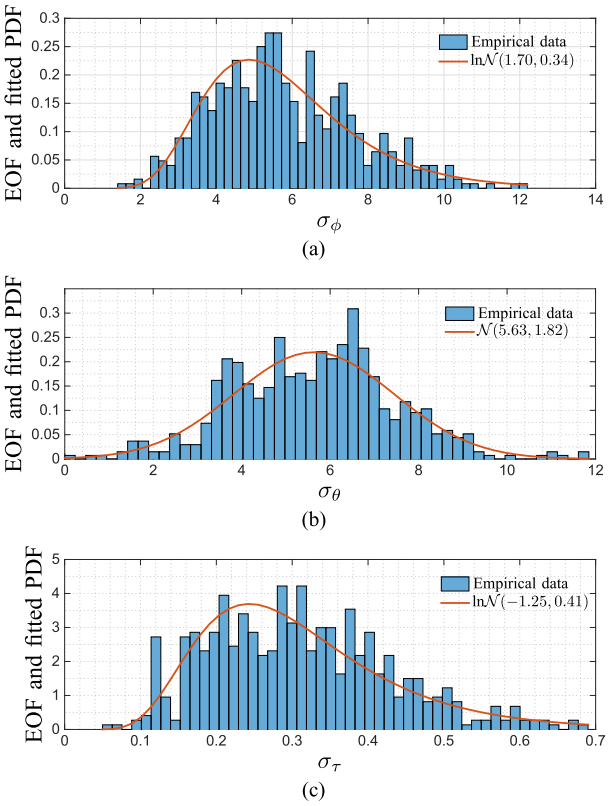

Fig. 9. **Empirical EOF and fitted PDFs for the AoA, ZoA and delay spreads of each cluster.**

TABLE 2. **A summary of the cluster statistical characteristics extracted from five measurements in the laboratory.**

Characteristics	Distributions identified			
Number of clusters	μ	96	σ	22
$P_i(\tau)$ [dB]	$P_i(\tau) = -0.52\tau - 64.37$			
σ_ϕ [ln(°)]	$\ln\mathcal{N}(1.70, 0.34)$*			
σ_θ [°]	$\mathcal{N}(5.63, 1.82)$			
σ_τ [ln(ns)]	$\ln\mathcal{N}(-1.25, 0.41)$			
$\rho_{\phi\theta}$	$\mathcal{L}(0.005, 0.18)$			
$\rho_{\phi\tau}$	$\mathcal{L}(-0.006, 0.30)$			
$\rho_{\theta\tau}$	$\mathcal{L}(0.146, 0.28)$			

* Notice that σ_ϕ in degrees corresponding to the value 1.70 in $\ln[°]$ is 5.4°.

frequency (EOF) and fitted probability density functions (PDFs) of the cluster AoA spreads σ_ϕ, ZoA spread σ_θ, delay spread σ_τ, and correlation coefficients $\rho_{\phi\theta}$, $\rho_{\phi\tau}$, $\rho_{\theta\tau}$ for the O2O channels. For the spreading parameters, either Normal distribution, denoted with $\mathcal{N}(\mu, \sigma)$, or log-normal distribution, denoted with $\ln\mathcal{N}(\mu, \sigma)$ are found to fit well with the empirical PDFs.

The values of those distribution parameters are provided in Table 2. For the correlation coefficients, the Laplace distribution denoted with $\mathcal{L}(\mu, b)$ where μ and b represent the location parameter and the scale parameter respectively, are found to fit well with the real PDFs. Furthermore, the number of clusters has the mean of 96 and standard deviation equal to 22. Table 2 reports the details of the model established for O2O channels. It is worth mentioning that by

TABLE 3. Model parameters reported in literature for HFB, mm-wave bands and sub-6 GHz bands for indoor or hall scenarios.

Parameters		2.35 GHz [48]	15 GHz (Here)	28 GHz [49]	60 GHz [35]	72 GHz [22]	3.1 – 10.6 GHz [50]
Antenna used		Array	10°	10°	18°	10°	Array
Number of clusters	μ	12	96	1.26	4	3	13
σ_ϕ [°]	μ	2.6	5.4	4.72	1.5	7	2.8*
	σ	1.3	1.4	2.69	-	3	-
σ_θ [°]	μ	-	5.63	-	-	5.7	-
	σ	-	1.82	-	-	2	-
σ_τ [ns]	μ	6.1	0.28	-	-	-	0.39*
	σ	-	0.31	-	-	-	-

*: Averaged with the values given in [50, Table II].

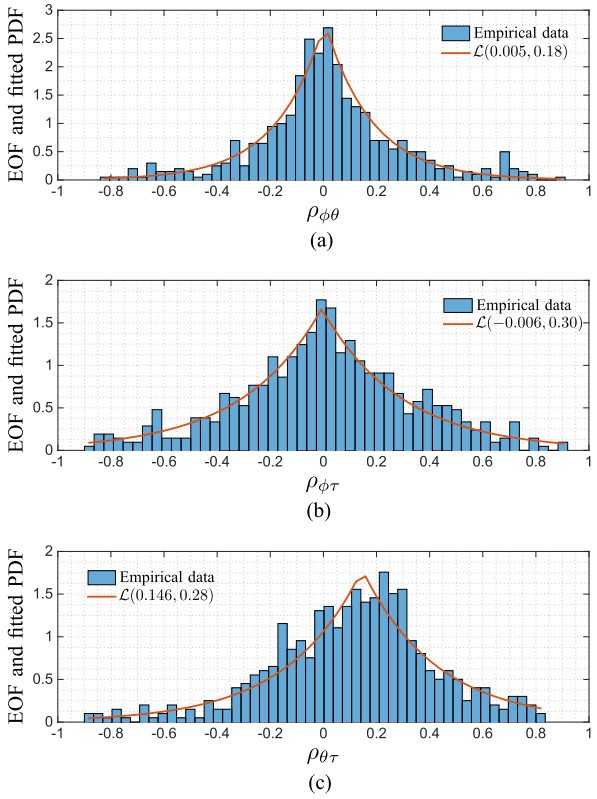

Fig. 10. Empirical EOF and fitted PDFs for the correlation coefficients between AoA, ZoA and delay of each cluster. (a) Correlation coefficients between AoA and ZoA. (b) Correlation coefficients between AoA and delay. (c) Correlation coefficients between ZoA and delay.

checking the AoA and ZoA spreads of LoS clusters observed in all measurements, we found that the antenna radiation pattern itself can induce a 5° angular spread. The observation in Table 2 that the mean AoA and ZoA spreads are slightly larger than 5° indicates that the clusters identified in our case are concentrated in angular domains, and each cluster may consist of just a single MPC.

Table 3 compares our cluster parameters to those given by literature in other HFBs. It is interesting to see that the cluster spreads in AoA and ZoA at 15 GHz are close to those reported in e.g. WINNER SCME [29] for indoor office environments below 6 GHz. Furthermore, the number of clusters in the 15 GHz O2O channels is significantly larger than those given in WINNER SCMEs and other measurements. This is consistent with the aforementioned observation that many clusters identified seem to contain a single MPC, due to the high resolutions in delay and angular domains in the measurements considered.

VI. CONCLUSIONS

In this contribution, a contrastive indoor channel measurement campaign for characterizing the differences of 15 GHz wave propagation channels for omnidirectional Tx and directive Tx scenarios was introduced. A practical method was proposed to extract clusters consisting of MPCs and diffuse scattering under some pre-defined settings for the maximum cluster size and the noise threshold. A drawback of this method is that the clustering results obtained are dependent on specific settings of these parameters. Clusters were extracted from the measured 3-dimensional power spectra in the azimuth of arrival (AoA), zenith of arrival (ZoA) and delay domains. The results showed that the channels observed in the omni-Tx to synthesized omni-Rx (O2O) and directional-Tx to synthesized omni-Rx (D2O) scenarios exhibit significant differences in e.g. the decaying slope of received power against delay, the richness of paths, and the behavior of dense multipath components. It was observed by mapping the clusters to interacting objects in the environment that most clusters were generated by single-bounce propagation. In addition, the statistics of the clusters for O2O channels were extracted based on five measurements. These results are important for validating channel models in ITU-R recommendations for higher frequency band wave propagation.

REFERENCES

[1] J. G. Andrews *et al.*, "What will 5G be?" *IEEE J. Sel. Areas Commun.*, vol. 32, no. 6, pp. 1065–1082, Jun. 2014.

[2] S. Salous *et al.*, "Millimeter-wave propagation: Characterization and modeling toward fifth-generation systems. [Wireless Corner]," *IEEE Antennas Propag. Mag.*, vol. 58, no. 6, pp. 115–127, Dec. 2016.

[3] T. Jämsä, P. Kyösti, and K. Kusume, "Deliverable d1.2 initial channel models based on measurements," document ICT-317669-METIS/D1.2, Mobile and wireless communications Enablers for the Twenty-twenty Information Society (METIS), 2014.

[4] J. Medbo *et al.*, "Channel modelling for the fifth generation mobile communications," in *Proc. 8th Eur. Conf. Antennas Propag. (EuCAP)*, Hague, The Netherlands, Apr. 2014, pp. 219–223.

[5] R. J. Weiler, M. Peter, and T. Kühne, M. Wisotzki, and W. Keusgen, "Simultaneous millimeter-wave multi-band channel sounding in an urban access scenario," in *Proc. Eur. Conf. Antenna Propag.*, Lisbon, Portugal, Apr. 2015, pp. 1–5.

[6] M. Kim, J.-I. Takada, Y. Chang, J. Shen, and Y. Oda, "Large scale characteristics of urban cellular wideband channels at 11 GHz," in *Proc. Eur. Conf. Antenna Propag. (EuCAP)*, Lisbon, Portugal, Apr. 2015, pp. 1–4.

[7] K. Belbase, M. Kim, and J.-I. Takada, "Study of propagation mechanisms and identification of scattering objects in indoor multipath channels at 11 GHz," in *Proc. Eur. Conf. Antenna Propag. (EuCAP)*, Lisbon, Portugal, Apr. 2015, pp. 1–4.

[8] T. S. Rappaport *et al.*, "Millimeter wave mobile communications for 5G cellular: It will work!" *IEEE Access*, vol. 1, pp. 335–349, May 2013.

[9] Y. Azar *et al.*, "28 GHz propagation measurements for outdoor cellular communications using steerable beam antennas in New York city," in *Proc. IEEE Int. Conf. Commun. (ICC)*, Jun. 2013, pp. 5143–5147.

[10] M. K. Samimi and T. S. Rappaport, "Ultra-wideband statistical channel model for non line of sight millimeter-wave urban channels," in *Proc. IEEE Global Commun. Conf. (GLOBECOM)*, Dec. 2014, pp. 3483–3489.

[11] M. K. Samimi and T. S. Rappaport, "Statistical channel model with multi-frequency and arbitrary antenna beamwidth for millimeter-wave outdoor communications," in *Proc. IEEE Global Commun. Conf., Exhibit. Ind. Forum (GLOBECOM) Workshop*, Dec. 2015, pp. 1–7.

[12] X. Wu, Y. Zhang, C.-X. Wang, G. Goussetis, E.-H. M. Aggoune, and M. M. Alwakeel, "28 GHz indoor channel measurements and modelling in laboratory environment using directional antennas," in *Proc. 9th Eur. Conf. Antennas Propag. (EuCAP)*, Apr. 2015, pp. 1–5.

[13] C. Gustafson, K. Haneda, S. Wyne, and F. Tufvesson, "On mm-wave multipath clustering and channel modeling," *IEEE Trans. Antennas Propag.*, vol. 62, no. 3, pp. 1445–1455, Mar. 2014.

[14] M. K. Samimi and T. S. Rappaport, "3-D millimeter-wave statistical channel model for 5G wireless system design," *IEEE Trans. Microw. Theory Techn.*, vol. 64, no. 7, pp. 2207–2225, Jul. 2016.

[15] Y. Ji, X. Yin, H. Wang, X. Lu, and C. Cao, "Antenna-de-embedded characterization for 13-17 GHz wave propagation in indoor environments," *IEEE Antennas Wireless Propag. Lett.*, vol. PP, no. 99, pp. 1–1.

[16] P. F. M. Smulders, "Statistical characterization of 60-GHz indoor radio channels," *IEEE Trans. Antennas Propag.*, vol. 57, no. 10, pp. 2820–2829, Oct. 2009.

[17] H. Sawada, H. Nakase, S. Kato, M. Umehira, K. Sato, and H. Harada, "Impulse response model and parameters for indoor channel modeling at 60GHz," in *Proc. IEEE 71st Veh. Technol. Conf. (VTC)*, May 2010, pp. 1–5.

[18] N. Moraitis and A. D. Panagopoulos, "Millimeter wave channel measurements and modeling for indoor femtocell applications," in *Proc. Eur. Conf. Antenna Propag.*, Lisbon, Portugal, Apr. 2015, pp. 1–6.

[19] A. Karttunen, K. Haneda, and J. Järveläinen, and J. Putkonen, "Polarisation characteristics of propagation paths in indoor 70 GHz channels," in *Proc. Eur. Conf. Antenna Propag.*, Lisbon, Portugal, May 2015, pp. 1–4.

[20] S. Nie, G. R. MacCartney, Jr., S. Sun, and T. S. Rappaport, "72 GHz millimeter wave indoor measurements for wireless and backhaul communications," in *Proc. IEEE 24th Int. Symp. Pers. Indoor Mobile Radio Commun. (PIMRC)*, Sep. 2013, pp. 2429–2433.

[21] V. Semkin, U. Virk, A. Karttunen, K. Haneda, and A. V. Räisänen, "E-band propagation channel measurements in an urban street canyon," in *Proc. Eur. Conf. Antenna Propag.*, Lisbon, Portugal, May 2015, pp. 1–4.

[22] N. Zhang, X. Yin, S. X. Lu, M. Du, and X. Cai, "Measurement-based angular characterization for 72 GHz propagation channels in indoor environments," in *Proc. Globecom Workshop-Mobile Commun. Higher Freq. Bands*, Dec. 2014, pp. 370–376.

[23] G. R. Maccartney, T. S. Rappaport, S. Sun, and S. Deng, "Indoor office wideband millimeter-wave propagation measurements and channel models at 28 and 73 GHz for ultra-dense 5G wireless networks," *IEEE Access*, vol. 3, pp. 2388–2424, 2015.

[24] T. S. Rappaport, G. R. Maccartney, M. K. Samimi, and S. Sun, "Wideband millimeter-wave propagation measurements and channel models for future wireless communication system design," *IEEE Trans. Commun.*, vol. 63, no. 9, pp. 3029–3056, Sep. 2015.

[25] J. Gozalvez, "Prestandard 5G Developments [Mobile Radio]," *IEEE Veh. Technol. Mag.*, vol. 9, no. 4, pp. 14–28, Dec. 2014.

[26] S. Hur, Y.-J. Cho, J. Lee, N.-G. Kang, J. Park, and H. Benn, "Synchronous channel sounder using horn antenna and indoor measurements on 28 GHz," in *Proc. IEEE Int. Black Sea Conf. Commun. Netw. (BlackSeaCom)*, May 2014, pp. 83–87.

[27] K. Haneda, J. Järveläinen, A. Karttunen, M. Kyrö, and J. Putkonen, "A statistical Spatio-Temporal radio channel model for large indoor environments at 60 and 70 GHz," *IEEE Trans. Antennas Propag.*, vol. 63, no. 6, pp. 2694–2704, Jun. 2015.

[28] *Technical Specification Group Radio Access Network; Spatial Channel Model for Multiple Input Multiple Output (MIMO) Simulations*, document 3GPP TR 25.996 V13.0.0, 3rd Generation Partnership Project, 2015.

[29] P. Kyosti *et al.*, *WINNER II Channel Models D1.1.2 V1.1*, European Commission, Deliverable IST-WINNER D, IST Winner II Project, Nov. 2007.

[30] X. Yin, and X. Cheng, *Propagation Channel Characterization, Parameter Estimation and Modeling for Wireless Communications*. Hoboken, NJ, USA: Wiley, 2016.

[31] B. H. Fleury, M. Tschudin, R. Heddergott, D. Dahlhaus, and K. I. Pedersen, "Channel parameter estimation in mobile radio environments using the SAGE algorithm," *IEEE J. Sel. Areas Commun.*, vol. 17, no. 3, pp. 434–450, Mar. 1999.

[32] B. H. Fleury, P. Jourdan, and A. Stucki, "High-resolution channel parameter estimation for MIMO applications using the SAGE algorithm," in *Proc. Int. Zurich Seminar Broadband Commun.*, vol. 30. Zürich, Switzerland, Feb. 2002, pp. 30-1–30-9.

[33] S. Sun, G. R. MacCartney, Jr., M. K. Samimi, and T. S. Rappaport, "Synthesizing omnidirectional antenna patterns, received power and path loss from directional antennas for 5G millimeter-wave communications," in *Proc. IEEE Global Commun. Conf. (GLOBECOM)*, Dec. 2015, pp. 1–7.

[34] D. Dupleich *et al.*, "Directional characterization of the 60 GHz indoor-office channel," in *Proc. 31th URSI General Assembly Sci. Symp.*, Beijing, China, Aug. 2014, pp. 1–4.

[35] A. Karttunen, J. Jarvelainen, A. Khatun, and K. Haneda, "Radio propagation measurements and WINNER II parameterization for a shopping mall at 60 GHz," in *Proc. IEEE 81st Veh. Technol. Conf. (VTC)*, May 2015, pp. 1–5.

[36] B. H. Fleury, "First- and second-order characterization of direction dispersion and space selectivity in the radio channel," *IEEE Trans. Inf. Theory*, vol. 46, no. 6, pp. 2027–2044, Sep. 2000.

[37] L. Materum, J.-I. Takada, I. Ida, and Y. Oishi, "Mobile station spatio-temporal multipath clustering of an estimated wideband MIMO double-directional channel of a small urban 4.5GHZ Macrocell," *EURASIP J. Wireless Commun. Netw.*, vol. 2009, 2009, Art. no. 9.

[38] N. Czink, P. Cera, J. Salo, E. Bonek, J. P. Nuutinen and J. Ylitalo, "A framework for automatic clustering of parametric MIMO channel data including path powers," in *Proc. IEEE Veh. Technol. Conf.*, Montreal, QC, Canada, 2006, pp. 1–5.

[39] N. Czink, "The random cluster model a stochastic mimo channel model for broadband wireless communication systems of the 3rd generation and beyond," Ph.D. dissertation, Techn. Univ. Wien, Vienna, Austria, 1979.

[40] A. A. M. Saleh and R. Valenzuela, "A statistical model for indoor multipath propagation," *IEEE J. Sel. Areas Commun.*, vol. 5, no. 2, pp. 128–137, Feb. 1987.

[41] A. Richter and R. S. Thoma, "Joint maximum likelihood estimation of specular paths and distributed diffuse scattering," in *Proc. IEEE 61st Veh. Technol. Conf. (VTC-Spring)*, vol. 1. Stockholm, Sweden, May 2005, pp. 11–15.

[42] A. Hammoudeh and D. Scammell, "Effect of receive antenna directivity on rms delay spread and coherence bandwidth for indoor millimetre wave mobile radio channels," in *Proc. 5th Eur. Pers. Mobile Commun. Conf.*, Apr. 2003, pp. 406–411.

[43] J. H. Kim, M.-W. Jung, and Y. Keun, "Antenna directivity effect on the delay spread at millimeter-wave," in *Proc. 13th Int. Conf. Adv. Commun. Technol. (ICACT)*, Feb. 2011, pp. 8–12.

[44] Y. He, X. Yin, Y. Ji, S. Lu, and M. Du, "Spatial characterization of coherence bandwidth for 72 GHz mm-wave indoor propagation channel," in *Proc. Eur. Conf. Antenna Propag.*, Lisbon, Portugal, May 2015, pp. 1–5.

[45] V. Degli-Esposti, D. Guiducci, and A. de'Marsi, P. Azzi, and F. Fuschini, "An advanced field prediction model including diffuse scattering," *IEEE Trans. Antennas Propag.*, vol. 52, no. 7, pp. 1717–1728, Jul. 2004.

[46] S. Hur *et al.*, "28 GHz channel modeling using 3D ray-tracing in urban environments," in *Proc. Eur. Conf. Antenna Propag.*, Lisbon, Portugal, May 2015, pp. 1–5.

[47] V. Degli-Esposti *et al.*, "Polarimetric analysis of mm-wave propagation for advanced beamforming applications," in *Proc. Eur. Conf. Antenna Propag.*, Lisbon, Portugal, May 2015, pp. 1–4.
[48] C. Huang, J. Zhang, X. Nie, and Y. Zhang, "Cluster characteristics of wideband MIMO channel in indoor hotspot scenario at 2.35GHz," in *Proc. IEEE 70th Veh. Technol. Conf. Fall (VTC)*, Sep. 2009, pp. 1–5.
[49] S. Hur *et al.*, "Wideband spatial channel model in an urban cellular environments at 28 GHz," in *Proc. 9th Eur. Conf. Antennas Propag. (EuCAP)*, Apr. 2015, pp. 1–5.
[50] K. Haneda, J. Takada, and T. Kobayashi, "Double directional ultra wideband channel characterization in a line-of-sight home environment," IEICE Trans. Fundam. Electron. Commun. Comput. Sci., vol. 88-A, no. 9, pp. 2264–2271, 2005.
[51] M. D. Baldé, S. Avrillon, C. Brousseau, D. Lemur, and B. Uguen, "Spatial scanner channel sounder for space diversity studies," in *Proc. 10th Eur. Conf. Antennas Propag. (EuCAP)*, Apr. 2016, pp. 1–3.
[52] B. Peng, S. Rey, and T. Kürner, "Channel characteristics study for future indoor millimeter and submillimeter wireless communications," in *Proc. 10th Eur. Conf. Antennas Propag. (EuCAP)*, Apr. 2016, pp. 1–5.
[53] M.-T. Martinez-Ingles *et al.*, "Polarimetric indoor measurements at 94 GHz," in *Proc. 10th Eur. Conf. Antennas Propag. (EuCAP)*, Apr. 2016, pp. 1–3.
[54] X. Yin, C. Ling, and M.-D. Kim, "Experimental multipath-cluster characteristics of 28-GHz propagation channel," *IEEE Access*, vol. 3, pp. 3138–3150, 2015.
[55] N. Tran, T. Imai, and Y. Okumura, "Measurement of indoor channel characteristics at 20 GHz band," in *Proc. Int. Symp. Antennas Propag. (ISAP)*, Nov. 2015, pp. 1–4.
[56] G. J. M. Janssen, P. A. Stigter, and R. Prasad, "Wideband indoor channel measurements and BER analysis of frequency selective multipath channels at 2.4, 4.75, and 11.5 GHz," *IEEE Trans. Commun.*, vol. 44, no. 10, pp. 1272–1288, Oct. 1996.
[57] A. I. Sulyman, A. Alwarafy, G. R. MacCartney, T. S. Rappaport, and A. Alsanie, "Directional radio propagation path loss models for millimeter-wave wireless networks in the 28-, 60-, and 73-GHz bands," *IEEE Trans. Wireless Commun.*, vol. 15, no. 10, pp. 6939–6947, Oct. 2016.

XUEFENG YIN received the bachelor's degree in optoelectronics engineering from the Huazhong University of Science and Technology, Wuhan, China, in 1995, and the M.Sc. degree in digital communications and the Ph.D. degree in wireless communications from Aalborg University, Denmark, in 2002 and 2006, respectively. From 2006 to 2008, he was an Assistant Professor in Aalborg University. In 2008, he joined Tongji University as an Associate Professor with the College of Electronics and Information Engineering, Shanghai, China. Since 2017, he was promoted to a Full Professor and serves as the Vice Dean of the college. His research interests include high-resolution parameter estimation for propagation channels, channel characterization and stochastic modeling for 5G wireless communications, radar signal processing and target recognition. He has authored about 100 technical papers and co-authored the book *Propagation Channel Characterization, Parameter Estimation and Modeling for Wireless Communications* (John Wiley and Sons Edition, 2016).

YILIN JI received the bachelor's degree in electronics science and technology and the master's degree in circuits and systems from Tongji University, China, in 2012 and 2016, respectively. Since 2016, he joined the Antenna and Propagation Group as a Research Assistant with the Faculty of Electronics Systems, Aalborg University, Denmark. His research interests are in the fields of propagation channel parameter estimation and stochastic modeling for the 5G communication systems.

HUA YAN received the bachelor's degree in electronic engineering and the Ph.D. in signal and information processing from the University of Electronic Science and Technology of China in 2004 and 2011, respectively. Since 2011, he joined Huawei Technologies Co., Ltd., as a Communication Engineer. His research interests include the channel modeling and physical layer technologies in 5G communication systems.